Reticulate collisional structure in boundary-driven granular gases

Yanpei Chen*
State Key Laboratory of Multiphase Complex Systems, Institute of Process Engineering, Chinese Academy of Sciences, Beijing 100190, China

Wei Wang†
State Key Laboratory of Multiphase Complex Systems, Institute of Process Engineering, Chinese Academy of Sciences, Beijing 100190, China and University of Chinese Academy of Sciences, Beijing 100049, People's Republic of China

(Received 11 April 2018; revised manuscript received 11 January 2019; published 30 October 2019)

We report a peculiar head-on collision network between two vibrating boundaries in experiments performed during a parabolic flight and in a laboratory using horizontal vibration. This structure is a new ordering, which is due to an orientation correlation between the relative position and velocity of any particle pair. It weakens the collision frequency and produces a long-range boundary effect. Moreover, we find the molecular chaos assumption is violated in a larger portion of the phase space. Using an anisotropic distribution model, we modify angular integration results and compare them to the results of the kinetic theory.

DOI: 10.1103/PhysRevE.100.042908

I. INTRODUCTION

Multiparticle collisions [1] and boundary effects are still challenges for rapid granular flows or others far from equilibrium systems. Such problems are topics of broad interest due to fundamental importance for polymer solution [2], self-propelled particles [3] and colloids [4], self-organizing granular system [5], granular liquid crystals [6], and many other areas. Though kinetic theory and hydrodynamics [7–10] have been developed well, the mechanism of boundary effects is still unclear. For example, the boundary heating mechanism influences various properties of a granular flow such as the velocity distribution shapes [11], the thermal convection [12], and even the equipartition of energy in granular mixtures [13]. It becomes more complicated when there are multiparticle collisions. The above two issues are taken together and studied in this paper by a boundary heated granular experiment in parabolic flights and additional ones in laboratory conditions.

To take above multiparticle collisions [1] and boundary effects into account, one needs correlation [14,15] to characterize the granular dynamics (i.e., the breakdown of molecular chaos [9]) caused by the excluded volume effects and the dissipative interaction [16,17]. For instance, multiparticle interactions are introduced to study high-order correlations (triplet pair correlations for the ring kinetic theory) or a new pair-correlation parameter g_Q [1,18,19] in a free cooling system. Likewise, to identify and quantify the boundary effect, we need to obtain the boundary characteristic length l_m (i.e., the local mean-free path near the boundary layer). These depend on analyzing spatial correlation scale.

Most works focus on the correlation of the homogeneous state based on fluctuating hydrodynamics [20,21] or the ring kinetic equation [18]. For example, randomly driven granular gases have been demonstrated to exhibit the various correlation in both experiments [22,23] and numerical simulations [14], where the short-range [14] and long-range position correlation [15] have been quantitatively predicted by employing mode coupling theory within the framework of isotropic hydrodynamics. However, the velocity autocorrelation function of the bulk regions is different from the one of the boundary regions in the dense granular flow of a silo [24]. The same is true of the spatial velocity correlation [24]. Moreover, this correlation is proved to be sensitive to the mechanism of energy injection [22]. These imply that the correlation in the boundary heated system is different from the homogeneous state.

The nonisotropic boundary heating would lead to the emergence of spatial inhomogeneity [25] and anisotropy [26]. It has been observed that various parameters the granular temperature [27], pressure tensor [28], energy dissipation [29], and local velocity distribution [30,31] are all anisotropic in such system. Such anisotropy [32] increases with the inelastic coefficient and particle number. In addition, the granular hydrodynamic theory agrees well with the simulation results when inelasticity is small [33]. But the same does not apply to great inelasticity [28]. Most impressively, previous experimental [34–36] and simulation [10,31] results show that velocity distributions change from a two-peak distribution near the boundary layer to a one-peak distribution in the central layer. The above two-peak (non-Gaussian) velocity distribution [10,31,35,36] implies that velocity [22,37] correlation exists. Based on the above two factors (anisotropy and correlation), we expect that the orientational correlation exists in the boundary heated granular system.

Besides, the orientational correlation in some other granular systems, e.g., the random granular packing [38,39], has also received much concern in recent years. The orientational correlation [40–42] between translations and rotations

*ypchen@ipe.ac.cn
†wangwei@ipe.ac.cn

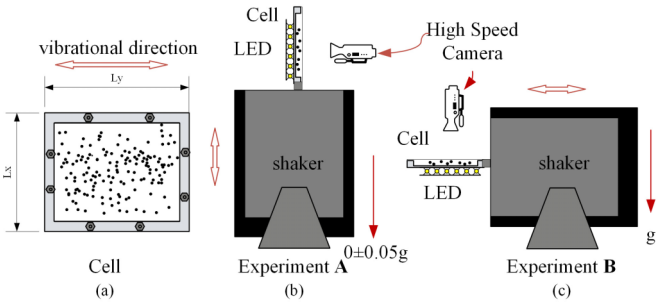

FIG. 1. Sketch of experiment. (a) a sample cell; (b) experimental apparatus of **A**; (c) experimental apparatus of **B**.

velocities has been found to exist even in a uniformly driven system. It is said to be responsible for the emergence of non-Gaussian high-velocity tails. Hence, it is of interest to ascertain if there is such orientational correlation in the boundary heated granular system and confirm its influence. It can improve the nonequilibrium dynamic description and be helpful to interpret attractors in the phase space [25].

In this paper, we report a multiparticle collision dynamic phenomenon occurring in boundary heated granular gases—collision particles forming a network between two vibrating walls. This reticulate structure is similar to the force chain in simple shear granular solids, but particles are long-running periods under contact. This hidden ordering is due to an orientation correlation between the relative position and velocity of any particle pair. We can describe this reticulate collision structure through a new parameter, the angular factor, β_m. The collision network can lead a multiparticle collision process, which is useful in a wide range of future applications for complex many-body systems.

II. EXPERIMENT DETAILS

We conduct two-dimensional vibrofluidized experiments combining results for two environments (Fig. 1). Spherical beads are held in a sample cell, which is mounted on a sinusoidal oscillation vibrator with the vibrational frequency f and maximum acceleration γ. Then the experiment is performed in two environments. The first experimental environment is the microgravity in parabolic flights of Novespace (denoted experiment **A**) with stable microgravity condition [0 ± 0.05 g, Fig. 1(b)] while the second is a laboratory subjected to a horizontal vibration [denoted experiment **B**, Fig. 1(c)]. The influence of gravity in both experiments **A** and **B** is neglected. Experimental parameters are listed in Table I. There are 47 bronze beads having various vibration strength in experiment **A**, area fraction $\Phi = N\pi d^2/(4L_xL_y) = 0.54$ (N is the total number of spheres with diameter d, L_x, and L_y are length and width of the cell, Φ defined as ratio of the area of particles to that of the cell). The particle number ranges from 16–272 in the experiment **B** under the same vibration. The movements of particles are recorded using a high-speed camera (at 499 and 500 frames per second in experiments **A** and **B**, respectively), and processed by IMAGEJ software with errors of around 10^{-4} m as shown in Table I. The detailed experimental settings of experiment **A** have been reported [35]. In the microgravity experiment, it is difficult to do experiments under different particle numbers, so experiment **B** conducted in the laboratory environment can be viewed as an additional experiment. We ignore the sliding and rolling friction in experiment **B**.

TABLE I. Summary of experimental parameters. d is the particle diameter, and L, W, and H are respectively the length, width, and height of the cell. R is the spatial resolution of the high-speed camera, given in pixels. f and is the vibrational frequency, and γ is the maximum acceleration.

		cell (mm)			R (pixels)		vibration	
Experiments	d (mm)	L	W	H	L	W	f (Hz)	γ (ms^{-2})
A	1.21	10	10	1.4	288	288	–	–
B	3	70	50	10	–	–	60	124

III. ORIENTATIONAL DISTRIBUTIONS

To begin, Fig. 2 first presents the radial-angular correlation distribution [43] $g(r, \theta)$ in microgravity experiment **A**, namely the density-density correlation function. Despite resembling a liquid structure [where the radial distribution function $g(r)$ is not shown here], $g(r, \theta)$ has two spikes along the vibrating direction, indicating anisotropy. In previous work [14], velocity-velocity correlation and position-velocity correlation are major concerns. Here, to identify the orientational correlation, we focus on the study of three relevant orientational probability distribution of: (i) the relative position $\hat{\boldsymbol{k}}$ between any two particles, $P(\alpha)$, (ii) their relative velocity $\boldsymbol{c}_{ij}$, $P(\boldsymbol{c}_{ij})$, and (iii) the angle between them, $\boldsymbol{c}_{ij} \cdot \hat{\boldsymbol{k}}$, $P(\Psi)$, as will be discussed, where $\hat{\boldsymbol{k}}$ is the unit vector directed from the center of particle i to that of j, and $\boldsymbol{c}_{ij}$ ($\boldsymbol{c}_{ij} = \boldsymbol{c}_i - \boldsymbol{c}_j$) the relative velocity. All these parameters are isotropic or uniform in

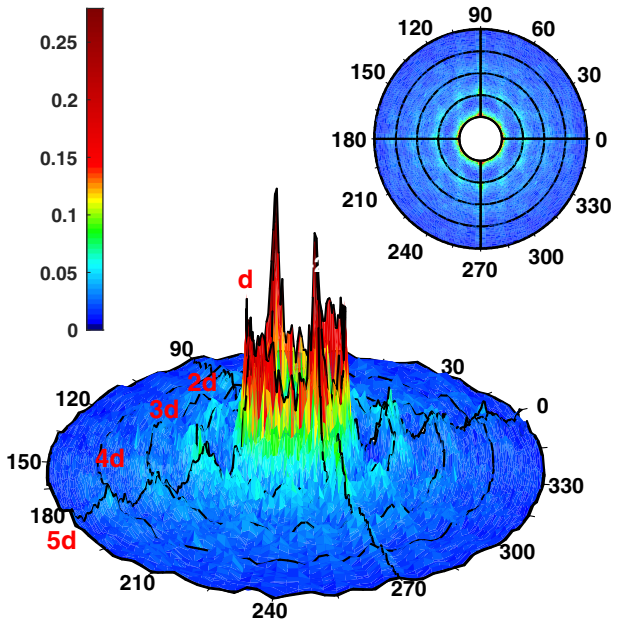

FIG. 2. Radial-angular correlation function $g(r, \theta)$ in microgravity, for which parameters are listed in Table I (**A**), at $f = 49$ Hz, and $\gamma = 21.6$ ms^{-2}.

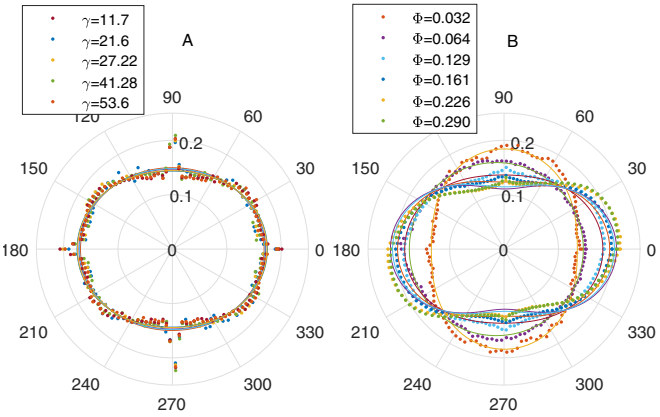

FIG. 3. Dependence of $P(\alpha)$ in experiment **A** on vibration acceleration [γ (ms^{-2}) = 11.7, 21.6, 27.22, 41.28, 53.6, f (Hz) = 49, 49, 97, 97, 97] and that in experiment **B** on the area fraction ($\Phi = 0.032$, 0.064, 0.129, 0.161, 0.226, 0.290) in polar coordinates. The maximum error in the levelness during the horizontal vibration experiment **B** is less than 0.5°. Other parameters are given in Table I.

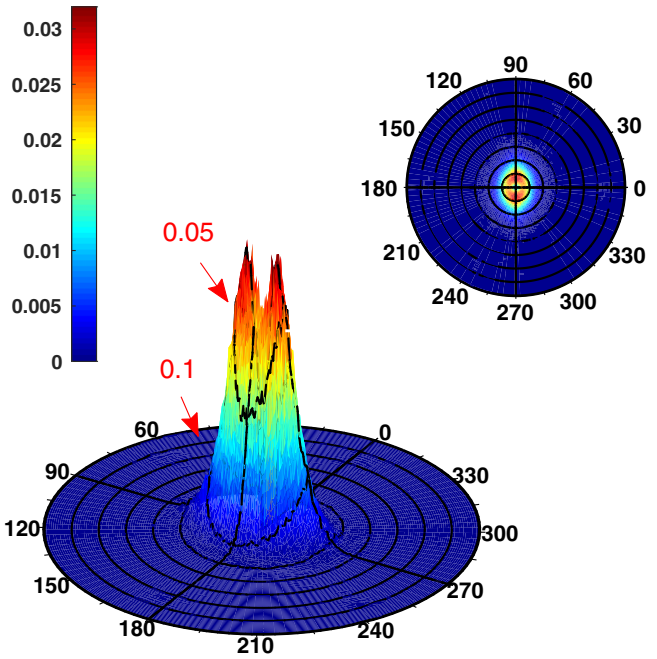

FIG. 4. Distribution function $P(\boldsymbol{c}_{ij})$ for relative velocity c_{ij} in experiment **A**. Experimental parameters are listed in Table I, f = 49 Hz and $\gamma = 21.6\ \mathrm{ms}^{-2}$.

classical kinetic theory. The circular distributions $P(\alpha)$ of $\hat{\boldsymbol{k}}$ in experiments **A** and **B** are shown in Fig. 3, where α is the angle of $\hat{\boldsymbol{k}}$. $P(\alpha)$ clearly has heterogeneity, in stark contrast with the case for uniform molecular gases, where $P(\alpha) = 1/2\pi$. Moreover, $P(\alpha)$ is flattened into an oblong shape along the y axis (the vibration direction). And its anisotropy increases proportionally with Φ. Nevertheless, $P(\alpha)$ slightly changes with γ. $P(\alpha)$ can be approximated using a truncated Fourier expansion as [44]

$$P(\alpha) = 1/2\pi[1 + a_1\cos(\alpha) + a_2\cos(2\alpha)], \qquad (1)$$

where a_1 and a_2 can be viewed as anisotropy parameters. This coupling model fits well, except failing to cover a few points near $\alpha = 0$, $\pi/2$, π, and $3\pi/2$ for experiment **A**. The reason is still unclear but the deviations present an orientational ordering.

Furthermore, the orientational distribution $P(\boldsymbol{c}_{ij})$ for experiment **A** is plotted in Fig. 4. Results of experiment **B** are similar to those in Fig. 4 and are not displayed here. For a molecular gas, $P(\boldsymbol{c}_{ij})$ is supposed to be isotropic and have a distribution $\sqrt{(2/\pi)}c_{ij}^2 e^{-1/2c_{ij}^2}$ [14]. However, $P(\boldsymbol{c}_{ij})$ in our cases is anisotropic and oval shaped with two peaks along the y axis, the vibration direction. This shape is due to the fact that particles gain maximum speed along the y axis ($\pi/2$ or $3\pi/2$) after colliding with the vibrating boundary. Then at the cell center, the particle velocity becomes more isotropic and lower, and the number density reaches a maximum. Therefore, the maximum of $P(\boldsymbol{c}_{ij})$ corresponds to the relative velocity between particles in the center layer and boundary layers, and $\boldsymbol{c}_{ij}$ is along the y axis.

We now turn to the circular distribution $P(\Psi)$, where Ψ is the angle between the relative velocity and relative position [22]; i.e., $\cos\Psi \equiv \boldsymbol{c}_{ij}\cdot\hat{\boldsymbol{k}}/|c_{ij}|$. We know that particles move away from each other (postcollision states) if $\cos\Psi$ is positive, and toward each other (precollision states) if $\cos\Psi$ is negative. For a fluidized granular fluid, Soto and Mareschal [45] derived a relation between the post- and precollision radial distribution functions at contact as a function of Ψ. But their model still takes isotropic Ψ of the precollision as an ansatz. We here plot $P(\Psi)$ of experiments **A** and **B** in Fig. 5. $P(\Psi)$ is not uniform. Furthermore, increasing γ or Φ leads to a flatter and more normal curve until there seems to be two plateaus. One is more likely to detect a postcollision state than a precollision state ($\pi/2 \leqslant \Psi \leqslant \pi$). This is similar to results for revised Enskog's factor χ derived by Soto and Mareschal [45] ($[\cos(\Psi)^2 + \alpha^2\sin(\Psi)^2]^{-1} > 1$ when $\alpha < 1$, where α is the restitution coefficient). For the randomly driven granular gases with Coulomb friction [46], $P(\Psi)$ increases in the range from $\pi/2$ to π. However, $P(\Psi)$ decreases in our case, except for the dilute condition ($\Phi = 0.032$). Note that $P(\Psi)$ here takes account of all particles pairs in our experiment, rather than Ψ near one particle diameter at contact. Hence, Ψ here is not a generalized pair correlation function at contact. We could also fit $P(\Psi)$ using a Fourier expansion,

$$P(\Psi) = 1/\pi[1 + c_1\cos(\Psi) + c_2\cos(2\Psi)]. \qquad (2)$$

The fitting results are plotted in Fig. 5. The dependence of c_1 and c_2 on Φ and γ are shown in the inset. Nonzero values of c_1 and c_2 clearly demonstrate that $P(\Psi)$ is anisotropic.

IV. CORRELATION AND ANGULAR FACTOR

We quantify the orientational correlation $\mathcal{M}$ as the mean square of the cosine of the angle Ψ', between $\boldsymbol{C}_{ij} = \boldsymbol{c}_{ij} - \langle\boldsymbol{c}_{ij}(t)\rangle$ and $\hat{\boldsymbol{K}} = \hat{\boldsymbol{k}} - \langle\hat{\boldsymbol{k}}(t)\rangle$:

$$\mathcal{M} = \left\langle \frac{1}{N}\sum_{i=1}^{N}\frac{(\boldsymbol{C}_{ij}\cdot\hat{\boldsymbol{K}})^2}{C_{ij}^2K^2}\right\rangle = \left\langle \frac{1}{N}\sum_{i=1}^{N}\cos^2\Psi'\right\rangle, \qquad (3)$$

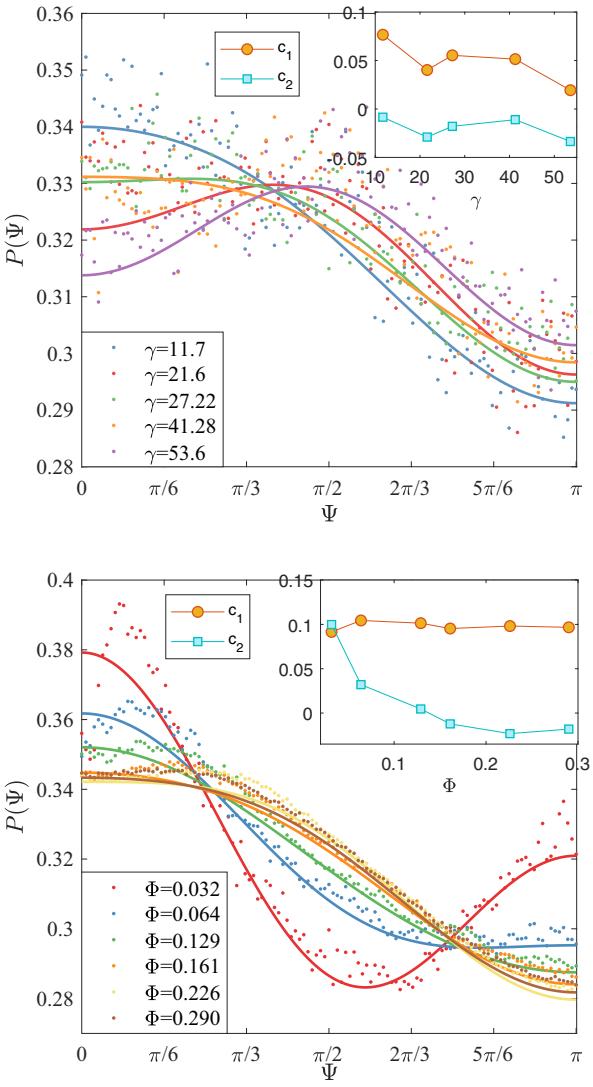

FIG. 5. Orientation distribution $P(\Psi)$ of experiments **A** (left) and **B** (right). The dashed line shows experimental results and the solid line shows fitting results obtained using Eq. (2). The inset shows the fitting coefficient versus Φ and γ.

where $\langle\rangle$ denotes an average (where $\langle \boldsymbol{c}_{ij}(t)\rangle$ and $\langle\hat{\boldsymbol{k}}(t)\rangle$ are averages taken over all particles in a frame, and the outermost brackets denote the average taken over all frames), and N is the total number of particles in each frame. If there is no correlation between $\hat{\boldsymbol{k}}$ and $\boldsymbol{c}_{ij}$, as in molecular gases, one obtains $\mathcal{M} = 1/2$. The evolutions of $\mathcal{M}$ with Φ and γ for experiments **A** and **B** are plotted as the inset of Fig. 6. $\mathcal{M}$ in both experiments **A** and **B** deviates from $1/2$ showing correlation between $\boldsymbol{c}_{ij}$ and $\hat{\boldsymbol{k}}$. $\mathcal{M}$ decreases monotonously with increasing Φ and remains relatively stable till $\Phi = 0.2$ for experiment **B**. It is interesting that the curve and the straight line $\mathcal{M} = 0.5$ intersect at around $\Phi = 0.13$. This is consistent with the previous experimental results [47] that the relative granular temperature drop $\triangle T/T_{\max}$ reaches a maximum at around $\Phi = 0.13$. This point is explained as a crossover from kinetic to collision transport of energy.

To further study $\mathcal{M}$, we also plot the probability distribution of $\cos\Psi'$ for experiment **B** in Fig. 6. There are two clear

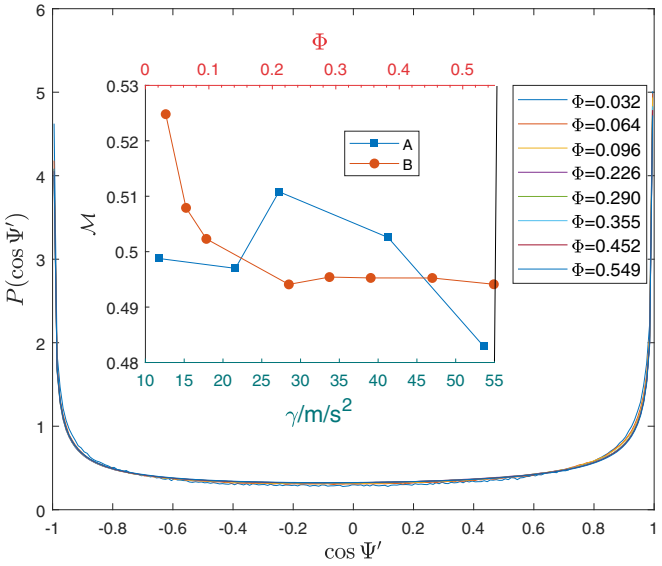

FIG. 6. Probability distribution of $\cos\Psi'$ of experiment **B** with vibrating parameters given in Table I. The inset shows $\mathcal{M}$ as a function of Φ or γ for experiments **A** and **B**.

peaks at $\cos\Psi' = -1$ and 1. The probability of the head-on collision is clearly higher than that of the oblique collision, which is consistent with the above and previous simulation results [48]. Inspired by Fig. 6, we draw lines between pairs of particles that satisfy $\cos\Psi' \in ([-1 \quad -0.9] \cup [0.9 \quad 1])$ and select the particles having the shortest separation, as shown in Fig. 7 and Fig. 8. In addition, the line width is

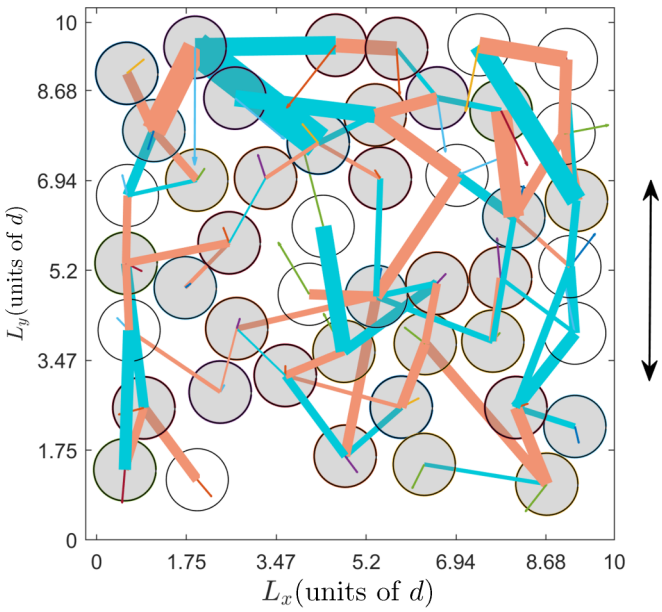

FIG. 7. Collision network for experiment **A**. Particles connected by light-coral lines satisfy $\cos\Psi' \in [-1 \quad -0.9]$ and those connected by cyan lines satisfy $\cos\Psi' \in [0.9 \quad 1]$. The line widths are proportional to the relative velocities. The arrow on each particle is a velocity vector. The vibration direction is shown by a double-headed arrow. d is the particle diameter. Gray particles are colliding and in contact with other particles.

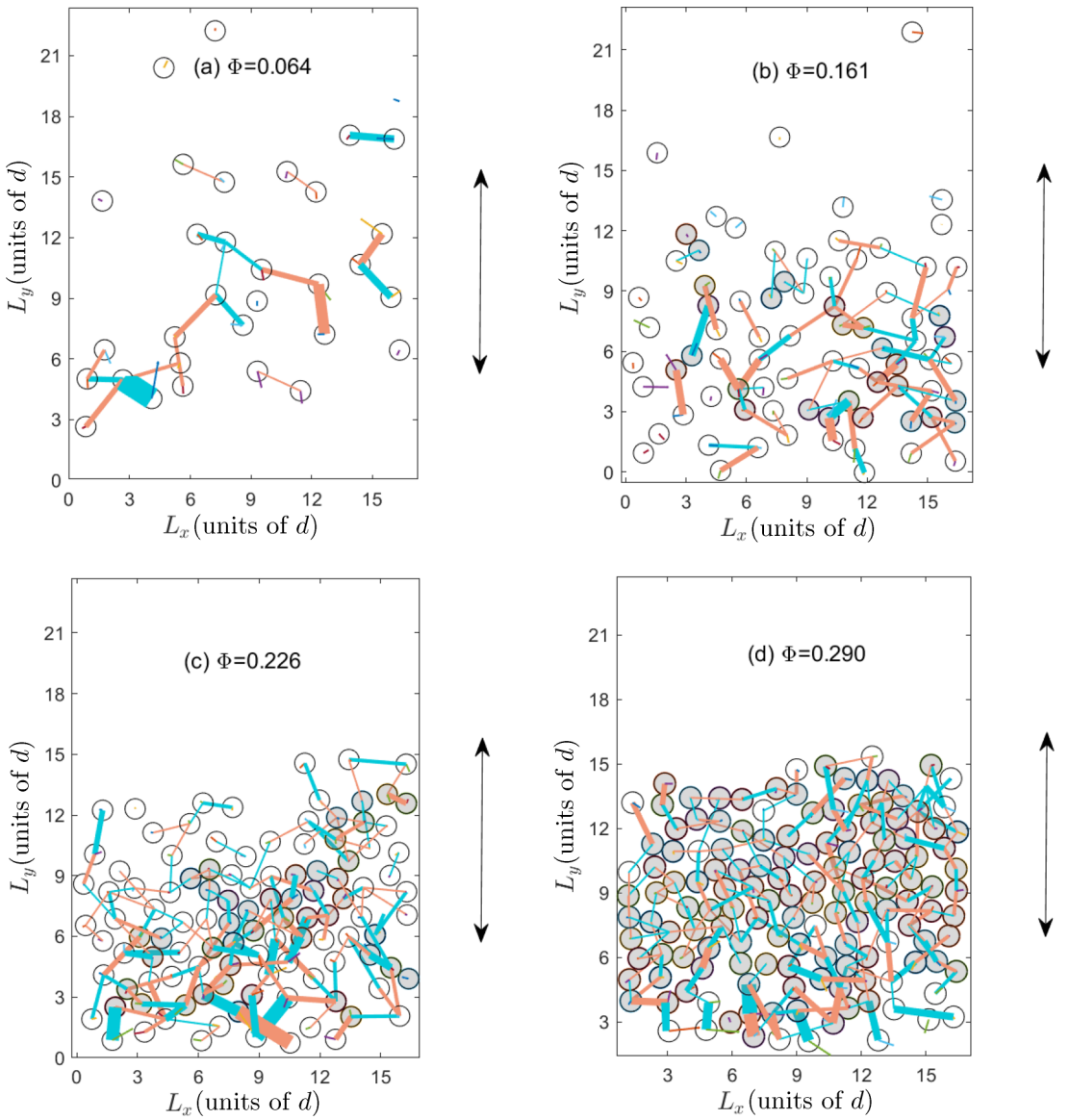

FIG. 8. Collision network for experiment **B**. (a) $\Phi = 0.032$; (b) $\Phi = 0.161$; (c) $\Phi = 0.226$; (d) $\Phi = 0.290$; Particles connected by light-coral lines satisfy $\cos\Psi' \in [-1 \quad -0.9]$ and those connected by cyan lines satisfy $\cos\Psi' \in [0.9 \quad 1]$. The line widths are proportional to the relative velocities. The arrow on each particle is a velocity vector. The vibration direction is shown by a double-headed arrow. d is the particle diameter. Gray particles are colliding and in contact with other particles.

drawn proportional to the relative velocity. All in-contact and head-on collision particle pairs are colored gray. As vividly depicted in figures, most particles have head-on collision relationships with their adjacent particles. There seems to be reticulate structures, connecting one particle to another between two driving boundaries, though the whole system seems homogenous. Let us define that a collision network consists of a set of particles within a boundary-driven rapid granular material that are held together and trapped by a network of head-on collisions. We emphasize that the network here is not limited in space but defined in the phase space with the position and velocity field. Fig. 7 and Fig. 8 also show this structure likely governs a large number of particles, in both dilute and dense cases.

To quantify effects of the anisotropic orientation on granular kinetic theory, a simple but practical method is defining a dimensionless angular integral, named the angular factor, as

$$\beta_m = \frac{\mathcal{J}_m}{\mathcal{J}_m^E} = \frac{\pi \int d\hat{\boldsymbol{k}}\Theta(-\hat{\boldsymbol{k}}\cdot\hat{\boldsymbol{g}})(\hat{\boldsymbol{k}}\cdot\hat{\boldsymbol{g}})^m P(\Psi)}{\int d\hat{\boldsymbol{k}}\Theta(-\hat{\boldsymbol{k}}\cdot\hat{\boldsymbol{g}})(\hat{\boldsymbol{k}}\cdot\hat{\boldsymbol{g}})^m}, \tag{4}$$

where $\hat{\boldsymbol{g}} \equiv \boldsymbol{c}_{ij}/c_{ij}$ is the unit vector directed along $\boldsymbol{c}_{ij}$, $P(\Psi)$ is the probability density distribution of Ψ, and Θ is the Heaviside step function. The denominator is the integral result corresponding to the evenly orientational distribution [49],

$$\mathcal{J}_m^E = \pi^{\frac{1}{2}} \frac{\Gamma\left(\frac{m+1}{2}\right)}{\Gamma\left(\frac{m+2}{2}\right)}. \tag{5}$$

It is known that the collision frequency, pressure, and energy dissipation contain the factor $|(\boldsymbol{c}_{ij}\cdot\hat{\boldsymbol{k}})^m| f^{(2)}(\mathbf{c}_i, \mathbf{c}_j, \hat{\boldsymbol{k}})$, where $f^{(2)}(\mathbf{c}_i, \mathbf{c}_j, \hat{\boldsymbol{k}})$ is the dynamic or constrained pair distribution function of velocities ($m = 1, 2, 3$). Therefore

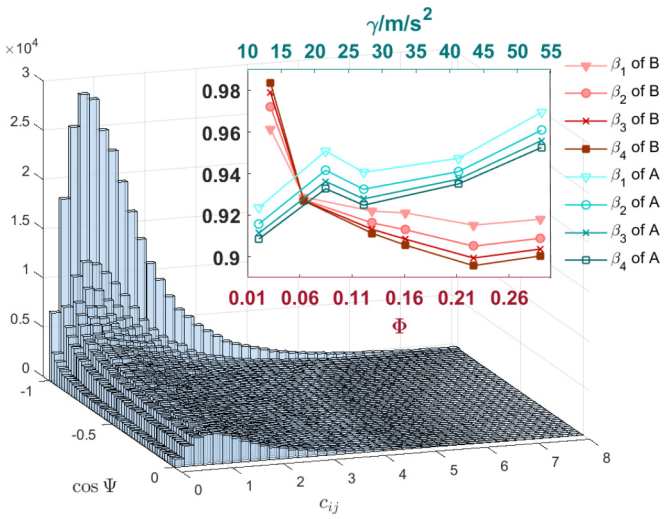

FIG. 9. The histogram of the c_{ij} and $\cos\Psi$ of **B** with $\Phi = 0.226$. Inset: Dimensionless angular integral β_m as a function of Φ and γ for experiments **A** and **B**.

$|\cos\Psi^m|$ is used to investigate the breakdown of the molecular chaos assumption. For randomly driven dissipated granular fluids [14], $\beta_m > 1$ and β_m approaches unity as m increases. In our case, we can introduce the anisotropy of Ψ [Eq. (2)] into β_m by applying our fitting parameters of $P(\Psi)$ in Eq. (2) to Eq. (4). Then β_m of experiments **A** and **B** are obtained, as illustrated by the inset of Fig. 9. We find that β_m also deviates from unity but $\beta_m < 1$. It means that, in boundary vibrofluidized granular gases, $|\cos(\Psi)|$ involved in the collision frequency is smaller than that in homogeneous state, so is $|\cos(\Psi)^3|$ involved in the energy dissipation. We know that the Enskog factor enhances the collision frequency at higher density. However, the emergence of this new chain structure weakens the collision frequency. It also means the local free path becomes longer, which is consistent with the previous results [1,48]. Besides the collision frequency, previous simulation results [50] show the dissipation rate decreases to $2/5$ of the theoretical prediction. Therefore our finding supports their assertion and first theoretically expound the reasons.

Besides, a previous study [51] defined high-frequency collision chains in dense granular flows and supposed uncorrelated in direction between $\hat{\boldsymbol{k}}$ and $\boldsymbol{c}_{ij}$. However, our results prove $\hat{\boldsymbol{k}}$ and $\boldsymbol{c}_{ij}$ are correlated in direction. And our chain structures are low-frequency collision chains. So it is a new structure. Furthermore, our results show that β_m deviates from unity more as m increases. This deviation increases with Φ and decreases with γ. That is because a larger vibration or lower density makes the system more homogeneous, with β_m being closer to 1. The variations of β_m imply that we can improve kinetic theory by introducing different $P(\Psi)$ for various boundary shapes. Unlike the method employing revised Enskog's factor [45] or dynamic velocity correlation [17], β_m accounts not only for spatial correlation but also for precollision position-velocity correlation [16].

Figure 9 is a histogram of c_{ij} and $\cos\Psi$ in the range of $\cos\Psi \in [-1 \quad 0]$ and for the relative distance $|\Delta \boldsymbol{r}_{ij}| < 2d$. For randomly driven granular fluids, one argument [14] is that the molecular chaos assumption only breaks down in a small portion of the phase space, where $|c_{ij}|$ is small and $\cos\Psi \to 0$. In Fig. 9, most data are located at $\cos\Psi \to -1$. So it is difficult to support that the molecular chaos assumption breaks down only at low relative velocity in our cases. It also demonstrates that the phase space of boundary heated granular gases is different from that of randomly driven gases.

V. CONCLUSION

In this paper, we found a remarkable multiparticle head-on network between two driving boundaries in boundary heated granular gases. Compared with previous aligning structure of the force chain, reticulate collision structure is a hidden order in configurations of the granular gases. It is caused by the orientation correlation between relative position and velocities. Even without the granular packing or cluster, the dynamical structure can appear in boundary-driven granular gases in the form of multiparticle collision networks. Considering the anisotropic orientation distribution of the relative position and velocities, we calculated the angular integration of the collision frequency, pressure, and the energy dissipation. Compared with integral results of isotropic angle distribution, it is found that results became smaller. Our findings demonstrate that the spatial velocity correlation is not enough. The orientation correlation between relative position and velocities also plays a crucial role in dissipative gases and cannot be neglected. Further studies of the collision network are likely to yield new insights about the granular kinetic theory with multiparticle collisions.

ACKNOWLEDGMENTS

The authors thank S. Luding, Y. J. Wang, and M. Hou for fruitful discussions. This work is supported by the Strategic Priority Research Program of Chinese Academy of Sciences (Grant No. XDA17010202), the National Natural Science Foundation of China under Grants No. 21625605, No. 11702291, and No. 21821005, the Fund of State Key Laboratory of Multiphase complex systems (Grant No. MPCS-2019-A-06). Y.C. was supported by grants from the Centre National d'Études Spatiales (France) and the Centre National de la Recherche scientifique (France).

[1] S. Luding, Nonlinearity **22**, R101 (2009).
[2] E. Falck, O. Punkkinen, I. Vattulainen, and T. Ala-Nissila, Phys. Rev. E **68**, 050102(R) (2003).
[3] L. F. Valadares, Y. Tao, N. S. Zacharia, V. Kitaev, F. Galembeck, R. Kapral, and G. A. Ozin, Small **6**, 565 (2010).
[4] R. G. Winkler, D. A. Fedosov, and G. Gompper, Curr. Opin. Colloid Interface Sci. **19**, 594 (2014).
[5] A. Deblais, T. Barois, T. Guerin, P. H. Delville, R. Vaudaine, J. S. Lintuvuori, J. F. Boudet, J. C. Baret, and H. Kellay, Phys. Rev. Lett. **120**, 188002 (2018).

[6] F. X. Villarruel, B. E. Lauderdale, D. M. Mueth, and H. M. Jaeger, Phys. Rev. E **61**, 6914 (2000).
[7] J. T. Jenkins and M. Y. Louge, Phys. Fluids **9**, 2835 (1997).
[8] I. Goldhirsch, Chaos **9**, 659 (1999).
[9] I. Goldhirsch, Annu. Rev. Fluid Mech. **35**, 267 (2003).
[10] J. J. Brey, M. J. Ruiz-Montero, and F. Moreno, Phys. Rev. E **62**, 5339 (2000).
[11] G. W. Baxter and J. S. Olafsen, Nature (London) **425**, 680 (2003).
[12] C. R. K. Windows-Yule, N. Rivas, and D. J. Parker, Phys. Rev. Lett. **111**, 038001 (2013).
[13] H. Wang and N. Menon, Phys. Rev. Lett. **100**, 158001 (2008).
[14] I. Pagonabarraga, E. Trizac, T. P. C. van Noije, and M. H. Ernst, Phys. Rev. E **65**, 011303 (2001).
[15] T. P. C. van Noije, M. H. Ernst, E. Trizac, and I. Pagonabarraga, Phys. Rev. E **59**, 4326 (1999).
[16] R. Soto, J. Piasecki, and M. Mareschal, Phys. Rev. E **64**, 031306 (2001).
[17] T. Pöschel, N. V. Brilliantov, and T. Schwager, Int. J. Mod. Phys. C **13**, 1263 (2002).
[18] T. P. C. V. Noije, M. H. Ernst, and R. Brito, Phys. A **251**, 266 (1998).
[19] O. Y. Sliusarenko, A. V. Chechkin, and Y. V. Slyusarenko, J. Math. Phys. **56**, 043302 (2015).
[20] J. J. Brey, F. Moreno, and M. J. Ruiz-Montero, Phys. Fluids **10**, 2965 (1998).
[21] K. Vollmayr-Lee, T. Aspelmeier, and A. Zippelius, Phys. Rev. E **83**, 011301 (2011).
[22] A. Prevost, D. A. Egolf, and J. S. Urbach, Phys. Rev. Lett. **89**, 084301 (2002).
[23] R. D. Wildman, J. P. Hansen, and D. J. Parker, Phys. Fluids **14**, 232 (2002).
[24] A. V. Orpe and A. Kudrolli, Phys. Rev. Lett. **98**, 238001 (2007).
[25] E. L. Grossman, T. Zhou, and E. Ben-Naim, Phys. Rev. E **55**, 4200 (1997).
[26] C. Scholz and T. Pöschel, Phys. Rev. Lett. **118**, 198003 (2017).
[27] D. V. D. Meer and P. Reimann, Europhys. Lett. **74**, 384 (2006).
[28] J. J. Brey and D. Cubero, Phys. Rev. E **57**, 2019 (1998).
[29] P. E. Krouskop and J. Talbot, Phys. Rev. E **69**, 061308 (2004).
[30] J. S. van Zon and F. C. MacKintosh, Phys. Rev. Lett. **93**, 038001 (2004).
[31] O. Herbst, P. Muller, M. Otto, and A. Zippelius, Phys. Rev. E **70**, 051313 (2004).
[32] W. Morgado and E. R. Mucciolo, Phys. A **311**, 150 (2002).
[33] J. Bougie, S. J. Moon, J. B. Swift, and H. L. Swinney, Phys. Rev. E **66**, 051301 (2002).
[34] C. Yanpei, P. Evesque, M. Hou, C. Lecoutre, F. Palencia, and Y. Garrabos, J. Phys.: Conf. Ser. **327**, 012033 (2011).
[35] Y. Chen, P. Evesque, and M. Hou, Chin. Phys. Lett. **29**, 074501 (2012).
[36] Y. Chen, M. Hou, Y. Jiang, and M. Liu, Phys. Rev. E **88**, 052204 (2013).
[37] G. W. Baxter and J. S. Olafsen, Phys. Rev. Lett. **99**, 028001 (2007).
[38] C. Xia, Y. Cao, B. Kou, J. Li, Y. Wang, X. Xiao, and K. Fezzaa, Phys. Rev. E **90**, 062201 (2014).
[39] Y. Jin, J. G. Puckett, and H. A. Makse, Phys. Rev. E **89**, 052207 (2014).
[40] N. V. Brilliantov, T. Pöschel, W. T. Kranz, and A. Zippelius, Phys. Rev. Lett. **98**, 128001 (2007).
[41] R. Rongali and M. Alam, Phys. Rev. E **89**, 062201 (2014).
[42] B. Gayen and M. Alam, Phys. Rev. Lett. **100**, 068002 (2008).
[43] I. I. H. Ansari and M. Alam, Phys. Rev. E **93**, 052901 (2016).
[44] F. Alonso-Marroquin, S. Luding, H. J. Herrmann, and I. Vardoulakis, Phys. Rev. E **71**, 051304 (2005).
[45] R. Soto and M. Mareschal, Phys. Rev. E **63**, 041303 (2001).
[46] O. Herbst, R. Cafiero, A. Zippelius, H. J. Herrmann, and S. Luding, Phys. Fluids **17**, 107102 (2005).
[47] N. D. Smith and M. I. Smith, Phys. Rev. E **96**, 062910 (2017).
[48] Y. Mei, Y. Chen, W. Wang, and M. Hou, Chin. Phys. B **25**, 084501 (2016).
[49] N. V. Brilliantov and T. Pöschel, *Kinetic theory of granular gases* (Oxford University Press, Oxford, 2010).
[50] S. McNamara and S. Luding, Phys. Rev. E **58**, 813 (1998).
[51] A. Ferguson and B. Chakraborty, Phys. Rev. E **73**, 011303 (2006).